

© 2024 IEEE Robotics and Automation Letters

Personal use of this material is permitted. Permission from IEEE Robotics and Automation Letters must be obtained for all other uses, in any current or future media, including reprinting or republishing this material for advertising or promotional purposes, creating new collective works, for resale or redistribution to servers or lists, or reuse of any copyrighted component of this work in other works.

Real-time Planning of Minimum-time Trajectories for Agile UAV Flight

Krystof Teissing*, Matej Novosad*, Robert Penicka, Martin Saska

Abstract—We address the challenge of real-time planning of minimum-time trajectories over multiple waypoints, onboard multirotor UAVs. Previous works demonstrated that achieving a truly time-optimal trajectory is computationally too demanding to enable frequent replanning during agile flight, especially on less powerful flight computers. Our approach overcomes this stumbling block by utilizing a point-mass model with a novel iterative thrust decomposition algorithm, enabling the UAV to use all of its collective thrust, something previous point-mass approaches could not achieve. The approach enables gravity and drag modeling integration, significantly reducing tracking errors in high-speed trajectories, which is proven through an ablation study. When combined with a new multi-waypoint optimization algorithm, which uses a gradient-based method to converge to optimal velocities in waypoints, the proposed method generates minimum-time multi-waypoint trajectories within milliseconds. The proposed approach, which we provide as open-source package, is validated both in simulation and in real-world, using Nonlinear Model Predictive Control. With accelerations of up to 3.5g and speeds over 100 km/h, trajectories generated by the proposed method yield similar or even smaller tracking errors than the trajectories generated for a full multirotor model.

Index Terms—Aerial Systems: Applications; Motion and Path Planning

SUPPLEMENTARY MATERIAL

Video: <https://youtu.be/wArd536Amro>

Code: https://github.com/ctu-mrs/pmm_uav_planner

I. INTRODUCTION

THE problem of finding a minimum-time trajectory for a multirotor Unmanned Aerial Vehicle (UAV) over multiple waypoints holds significant importance for various applications such as search and rescue [1], inspection and monitoring missions [2], and drone racing [3]. Finding a trajectory with minimal computational effort is crucial to enable real-time replanning during flight, even on less powerful flight computers used on small multirotors. The challenge lies in the need to solve a nonlinear optimization problem onboard in real-time. Achieving a truly time-optimal trajectory, as demonstrated in previous research, requires many hours [4] of computation, or at least several seconds [5], [6].

Manuscript received: July, 1, 2024; Revised August, 28, 2024; Accepted September, 19, 2024. This paper was recommended for publication by Editor G. Loianno upon evaluation of the Associate Editor and Reviewers' comments.

The authors are with the Multi-robot Systems Group, Faculty of Electrical Engineering, Czech Technical University in Prague, Czech Republic (<http://mrs.felk.cvut.cz/>). This work has been supported by the Czech Science Foundation (GAČR) under research project No. 23-06162M, by the European Union under the project Robotics and advanced industrial production (reg. no. CZ.02.01.01/00/22_008/0004590), and by CTU grant no SGS23/177/OHK3/3T/13.

Digital Object Identifier (DOI): see top of this page.

*These authors contributed equally to this work.

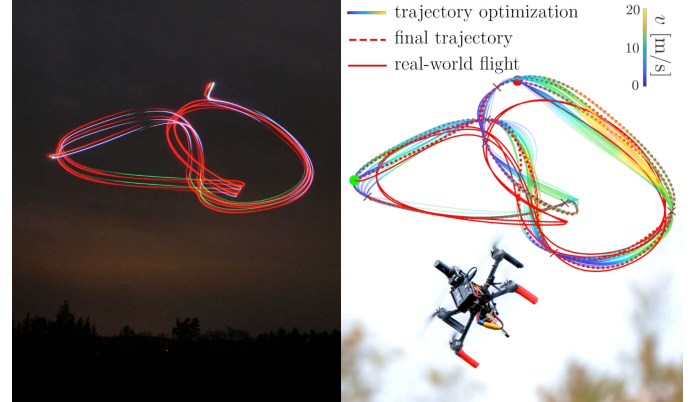


Fig. 1. Long exposure shot of real-world flight (left) and used UAV together with the visualization of trajectory optimization process (right).

Existing works on online trajectory planning often utilize polynomial [7] or B-spline [8] trajectory representations to compute smooth trajectories efficiently; however, they do not yield minimum-time trajectories due to their smoothness. Time-optimal trajectories have been found for a full dynamical model of a multirotor using computationally demanding methods [4], [9], or with sampling-based methods [10], [11] that solve the task for a double integrator acceleration-limited point-mass model (PMM). The PMM models only the translational motion of the UAV while ignoring rotational dynamics. Yet PMM allows for efficient trajectory planning suitable for real-time applications. However, even with this model, the sampling-based methods could compute trajectories with only a limited number of waypoints in real time. Additionally, existing approaches utilizing PMM apply per-axis acceleration constraints, which restrict the UAV's ability to utilize its maximum collective thrust. Moreover, for distant waypoints, PMM trajectories reaching high speeds may result in large tracking errors without accurate drag modeling, an issue that is yet to be addressed in PMM planning.

To address these limitations, we present a novel approach, which, within milliseconds, is able to generate minimum-time trajectories over multiple waypoints that can be tracked by a Nonlinear Model Predictive Controller (NMPC) with minimal tracking error. We constrain the acceleration norm, optionally also velocity, rather than limiting them per-axis. Constraining the norm enables us to use the maximum collective thrust of the drone and generate trajectories that are over 20% faster, compared to the existing works that use multiple, but non-flexible per-axis constraints [12]. We also directly consider gravitational force to fully utilize the collective acceleration produced by the propellers, avoiding conservative acceleration limits. The model is further refined by incorporating a linear

drag model. This is crucial when planning trajectories between distant waypoints, as minimum-time trajectories can reach extreme velocities, resulting in significant drag forces that, if disregarded, could lead to large tracking errors or even tracking failures. To the best of our knowledge, this is the first work to incorporate drag modeling into the PMM. The critical impact of described principles is demonstrated through an ablation study. We further introduce a novel gradient-based algorithm for multi-waypoint trajectory optimization, visualized in Fig. 1, which optimizes apriori unknown velocities at the waypoints and converges to optimal solutions 100 times faster than the sampling-based approach [11]. This is achieved by deriving the key objective function and optimization constraints necessary for fast and successful convergence, which are found in closed form. We verify our approach in real-flight outdoor experiments (see Fig. 1) by tracking trajectories with maximum thrust of up to 3.5g and velocities reaching over 100 km/h using a NMPC. Trajectories generated by our method within few milliseconds resulted in similar or even smaller tracking errors than the time-optimal trajectories requiring several hours of computation for a full quadrotor model [4]. We have open-sourced the method to be used by the community.

II. RELATED WORK

Several different methods have been used for trajectory planning for agile UAV flight where both computational time and time optimality are of critical importance. In [7], [13], [8], the authors utilize the concept of representing a UAV trajectory by continuous-time polynomials to achieve real-time capability. This representation is enabled by the differential flatness property [14] of a multirotor UAV, where all UAV states and inputs can be expressed using flat outputs and their finite number of derivatives. Obtaining derivatives of polynomials is computationally effective, which allows for fast computational times. Quadratic programming is used in [7] to find a polynomial trajectory, which is then optimized with respect to minimal snap and trajectory duration. Polynomial interpolation using piece-wise polynomial function called B-spline [13] followed by an optimization process combining multiple criteria to achieve perception-aware trajectory is used in [8]. However, in both cases, the inherent smoothness of polynomials prevents rendering time-optimal policies with rapid input changes. Direct collocation methods [6] achieve near-optimal performance by utilizing polynomials to approximate input and state dynamics, with computation times in the range of tens of seconds. A recently published approach [15] has reduced the computational time to seconds, but achieve only close-to-time-optimal results.

Time optimal maneuvers were planned in [16], but only in 2D. Time-optimal 3D trajectory planning for a full dynamical model of a multirotor has been introduced in [4], where a time allocation and a full state are assigned for all waypoints using a discretized dynamic model of the multirotor within a complex optimization process. The authors also address the coupling of linear and rotational acceleration given by the multirotors' design, which is not always addressed in state-of-the-art trajectory planning methods. Due to the complexity

of the proposed approach, the computational time can take several hours, depending on the number of waypoints. Yet, authors in [5] achieved reduction in runtime to just seconds.

To reduce the complexity of trajectory planning for a non-linear and high-dimensional model of a multirotor [17], the approaches [17], [18], [12], [10], [9], and [11] use a PMM approximation to generate trajectory, which can then be used to guide recent control methods [19] or further trajectory planning for full dynamical model [17], [10]. Pontryagin's maximum principle [20] is used to achieve a time-optimal PMM trajectory, which results in a bang-bang policy in the case of limited acceleration trajectories [17] and a bang-singular-bang policy for limited acceleration and velocity [18]. In [18], bang-singular-bang policy PMM trajectory generation was used under the Kinematic Orienteering Problem. The enhancement of their methodology was demonstrated in [12], where four per-axis cases for velocity and acceleration constraints were introduced. However, the assumption of known full states at all waypoints makes the method unsuitable for multi-waypoint trajectories. The authors of [10] also use bang-singular-bang trajectories but solve the ambiguity for multi-waypoint trajectories by sampling different velocity vectors at each waypoint. The minimum duration trajectory is then fitted with a polynomial, retaining thus the previously mentioned drawbacks. Limited acceleration PMM trajectory planning was implemented in [17] within an obstacle avoidance framework. However, no axis synchronization was addressed. The ability of modern control methods to track infeasible but differentiable paths was demonstrated in [9], [11], where a Model Predictive Contouring Control [19] method is used to track PMM bang-bang trajectories. Similar to [10], the ambiguity in velocities for multi-waypoint trajectories is solved by generating gradually adjusted velocity samples from inside a cone; the samples that result in the shortest trajectory duration are selected. In [9], a gradient descent method on a sphere was added to optimize the thrust decomposition and solve the problem of coupled rotational and linear acceleration of a multirotor, obtaining thus the minimum-time trajectories. However, as the computational complexity of this method grows quadratically with the number of samples per waypoint, a receding horizon approach had to be used in a real-time replanning application [11], where the trajectory was generated only for few subsequent waypoints. Our method can converge to optimal solutions 100 times faster thanks to continuous velocity optimization.

While PMM effectively reduces the complexity of planning by neglecting rotational dynamics including the heading, theoretically optimal trajectories are not feasible since they require infinite angular acceleration to change the direction of thrust instantaneously. The infeasibility and heading ambiguity can be resolved by using NMPC, which accounts for the vehicle's rotational dynamics and physical constraints, and can track infeasible trajectories with errors comparable to trajectories planned for full dynamical model.

III. METHODOLOGY

A. Time-Optimal Point-Mass Model Trajectory Planning

For a PMM trajectory segment Π with limited acceleration resulting in a bang-bang policy, we define the start and end state as positions $\mathbf{p}_0, \mathbf{p}_2 \in \mathbb{R}^n$ and velocities $\mathbf{v}_0, \mathbf{v}_2 \in \mathbb{R}^n$, where n is the dimensionality of the space in which the trajectory is computed; $n = 3$ for our application. The control input is the acceleration $\mathbf{a} \in \mathbb{R}^n$ in the world frame, which is bounded by the per-axis acceleration limits $\mathbf{a}_{\min}, \mathbf{a}_{\max} \in \mathbb{R}^n \setminus \{0\}$, where the j -th component of \mathbf{a} holds $a_{\min}^j \leq a^j \leq a_{\max}^j$, $j = 1, \dots, n$. We also consider $\mathbf{a} \neq \mathbf{0}$ for a non-zero trajectory with $\mathbf{p}_0 \neq \mathbf{p}_2$. Without loss of generality, we define a single-axis trajectory segment first. Given the Pontryagin's maximum principle [20], a time-optimal PMM trajectory segment can be described as:

$$\begin{aligned} p_1 &= p_0 + v_0 t_1 + \frac{1}{2} a_1 t_1^2, & v_1 &= v_0 + a_1 t_1, \\ p_2 &= p_1 + v_1 t_2 + \frac{1}{2} a_2 t_2^2, & v_2 &= v_1 + a_2 t_2, \end{aligned} \quad (1)$$

where $p_0, v_0 \in \mathbb{R}$ and $p_2, v_2 \in \mathbb{R}$ are the start and end states, $t_1, t_2 \in \mathbb{R}$ are the time durations of the corresponding sub-segments of the trajectory and

$$a_i \in \{a_{\min}, a_{\max}\}, \quad i = 1, 2, \quad a_i \in \mathbb{R}, \quad (2)$$

are the optimal control inputs. We omit the case where $a_1 = a_2$ as this is equivalent to $t_1 = 0$ or $t_2 = 0$, which leaves us with two combinations of possible values for a_1 and a_2 . Given the start state, end state, and limits on the acceleration, the unknowns are the sub-segment durations t_1, t_2 , velocity v_1 and position p_1 at time $t = t_1$. It can be shown that analytical solutions to the equations (1) exist and that there are four solutions in total; for each combination of a_1 and a_2 values, there are two. From those, the final solution is chosen such that all unknowns are real numbers, and the real-world condition of non-negative times $t_1 \geq 0$ and $t_2 \geq 0$ is satisfied. The total trajectory duration of the selected time-optimal solution is

$$T_{\text{ax}} = t_1 + t_2. \quad (3)$$

The bang-bang policy is impractical for longer distances between waypoints, as the resulting high velocities induce drag forces greater than the UAV can counteract. Therefore, we introduce an optional velocity limit $v_m > 0$, $|v(t)| \leq v_m$ for $t \in [0, T_{\text{ax}}]$. The time-optimal control inputs for bang-singular-bang policy are

$$a_i \in \{a_{\min}, 0, a_{\max}\}, \quad i = 1, 2, 3, \quad a_i \in \mathbb{R}, \quad (4)$$

with notation analogous to (1). If the speed limit is reached, the value of v_1 is known and equal to the maximum velocity $\pm v_m$. Then, an additional equation $p_\sigma = p_1 + v_m t_\sigma$, is added to the system (1), where the two new unknowns are the duration t_σ during which the acceleration $a_i = 0$ is applied, and the position p_σ at which the zero acceleration segment ends. It can be shown that the solution for all unknowns can be found in closed form. The total trajectory duration for the bang-singular-bang policy trajectory segment is then

$$T_{\text{ax}} = t_1 + t_\sigma + t_2. \quad (5)$$

B. Trajectory Axis Synchronization

The issue of generalizing the introduced concept of PMM trajectory to a multidimensional trajectory leads to the problem of axis synchronization. The time-optimal trajectory durations $T_{\text{ax}_1}, \dots, T_{\text{ax}_n}$ (as defined in equation (3) or (5)) for all n axes need to be synchronized to a common duration T_s . We follow the approaches [10] and [11], where T_s is set to the duration of the slowest per-axis trajectory and acceleration scaling factor $\gamma \in (0, 1]$, different for each axis, is used for scaling down the accelerations in the rest of the axes to prolong their duration. By substituting $\gamma_i a_i$ for both a_1 and a_2 in (1) and adding the condition of the set trajectory duration $T_s = t_1 + t_2$, one can obtain the solution for all unknowns in closed form. We select the solution where all unknowns are real numbers, time is non-negative, and γ is within the defined interval. However, such a solution does not necessarily exist as described in [12] since the correct position has to be integrated using the scaled accelerations in the given time. If no solution was found, the new feasible synchronization duration T_{snew} is computed. This is done by setting $\gamma = 1$ and solving (1) for the given axis. The feasible solution, for which T_{ax} is the shortest and $T_{\text{ax}} > T_s$ holds, is selected as the next synchronization duration. This is equivalent to obtaining the edge value of the nearest interval of feasible T_{ax} values, which are directly determined by the edge values of $\gamma \in (0, 1]$. We solve only for $\gamma = 1$ as $\gamma \rightarrow 0$ yields $T_{\text{ax}} \rightarrow \infty$. Given the T_{snew} , the synchronization is performed for all the remaining axes as described above. We refer to the above-described method for a synchronized one-segment multidimensional PMM trajectory as **pmmTraj3D** in Alg. 1 and Alg. 2.

C. Limited Thrust Decomposition (LTD)

Until now, we used per-axis acceleration limits. Yet, the unique property of multirotors is the coupling of the three-axis accelerations with the collective thrust vector produced by the motors with propellers. Additionally, external forces such as gravity and aerodynamic drag induced by fast flight need to be considered. To this end, we propose the following approach. Given a maximum collective thrust force f_{max} that the motors of a multirotor with mass m can produce, we compute its thrust acceleration \mathbf{a}^T limit as $a_{\text{max}}^T = f_{\text{max}}/m$. The acceleration \mathbf{a} of a trajectory must then for all times $t \in [0, T_s]$ satisfy the constraint

$$\|\mathbf{a}^T(t)\| = \|\mathbf{a}(t) - \mathbf{d}(t) - \mathbf{g}\| \leq a_{\text{max}}^T, \quad (6)$$

scheme where $\mathbf{g} = [0, 0, -g]^T$ and $\mathbf{d} = [-d^x, -d^y, -d^z]^T$ are gravitational and drag acceleration vectors, respectively.

Rather than deriving a complex optimization approach to solve the non-linear constraint (6), and to minimize the computational time, we build on the work [9] and iteratively approximate an optimal distribution of accelerations to minimize the T_s of a PMM trajectory segment.

For a single three-dimensional bang-bang policy trajectory segment with per-axis trajectory equations (1), the problem

can be formulated as

$$\begin{aligned} \{\mathbf{a}_1^*, \mathbf{a}_2^*\} &= \arg \min_{\mathbf{a}_1, \mathbf{a}_2 \in \mathbb{R}^3} T_{\Pi}(\mathbf{a}_1, \mathbf{a}_2) \\ \text{s.t. } a_i(t) &= a_1^i \text{ for } t \in [0, t_1^i], \text{ for } i \in \{x, y, z\}, \\ a_i(t) &= a_2^i \text{ for } t \in [t_1^i, T_{\Pi}], \text{ for } i \in \{x, y, z\}, \\ \|\mathbf{a}(t) - \mathbf{d}(t) - \mathbf{g}\| &\leq a_{\max}^T, \text{ for } t \in [0, T_s], \end{aligned} \quad (7)$$

where $\mathbf{a}_1 = [a_1^x, a_1^y, a_1^z]^\top$, $\mathbf{a}_2 = [a_2^x, a_2^y, a_2^z]^\top$, and T_{Π} is a function assigning the duration of a synchronized trajectory defined in Sec. III-B to the selected accelerations.

The duration of the first sub-segment for the i -axis t_1^i is referred to as acceleration switch time, and T_s is the total trajectory duration, solution to Sec. III-B. To approximate the solution to (7), we first decompose the maximal thrust a_{\max}^T into per-axis limits \mathbf{a}_{\max} and \mathbf{a}_{\min} by solving (6) for $a_{\text{init}} = a^x = a^y = a^z$ given that $\|\mathbf{a}^T\| = a_{\max}^T$. We also consider $\mathbf{d} = \mathbf{0}$ for this initialization step as the velocities necessary for drag estimation need to be computed first. This can be done in closed form with two solutions, from which we select the positive number. The initial per-axis acceleration limits are computed as

$$\begin{aligned} \mathbf{a}_{\max} &= \mathbf{a}_{\text{init}}^T + \mathbf{g} = [a_{\text{init}}, a_{\text{init}}, a_{\text{init}}]^\top, \\ \mathbf{a}_{\min} &= -\mathbf{a}_{\text{init}}^T + \mathbf{g} = -\mathbf{a}_{\max} + 2\mathbf{g}, \end{aligned} \quad (8)$$

where $\mathbf{a}_{\text{init}}^T$ is the initial thrust acceleration.

Using these values, we compute the multidimensional trajectory as described in Sec. III-B. As synchronizing trajectories are computed using acceleration downscaling, the acceleration norm will generally be smaller than a_{\max}^T throughout the trajectory segment. According to Pontryagin's maximum principle [20], the maximal acceleration is required to obtain time optimality. For our case, a thrust acceleration vector \mathbf{a}^T must at some point in time satisfy

$$\|\mathbf{a}^T\| = a_{\max}^T. \quad (9)$$

Using the bang-bang policy, we have three different per-axis switch times $t_1^i, i \in \{x, y, z\}$ which lead to four different thrust acceleration vectors $\mathbf{a}_l^T, l \in 1, \dots, 4$ in one segment. Using a linear drag model used in [21], drag vector \mathbf{d} is approximated for the most adverse scenarios for each \mathbf{a}_l , guaranteed to be right before per-axis switch times, as

$$\mathbf{d}_l = \mathbf{R}(t_l) \mathbf{D} \mathbf{R}^\top(t_l) \cdot \mathbf{v}(t_l), \quad (10)$$

where rotation matrix $\mathbf{R}(t)$ can be obtained from current acceleration, $\mathbf{D} = \text{diag}(\delta^x, \delta^y, \delta^z)$ is a diagonal matrix containing drag coefficients for each axis, and $t_l \in \{t_1^x, t_1^y, t_1^z, T_s\}$. In these instances, velocity is either maximized during acceleration, resulting in the largest drag acting opposite acceleration, or minimized during deceleration, with the smallest drag aligned in the same direction as the acceleration vector. Thus, over the duration of the trajectory, we observe four local maxima for thrust acceleration

$$\|\mathbf{a}_l^T\| = \|\mathbf{a}_l - \mathbf{d}_l - \mathbf{g}\|, \quad l \in \{1, \dots, 4\}. \quad (11)$$

To find the per-axis acceleration limits \mathbf{a}_{\max} and \mathbf{a}_{\min} which result in satisfying the condition (9) for all thrust accelerations \mathbf{a}_l^T , we propose the following iterative approach. In each step,

all \mathbf{a}_l^B are scaled by their unique factors β_l to achieve (9). The factors are computed by solving the equation

$$a_{\max}^T = \|\beta_l \mathbf{a}_l - \mathbf{d}_l - \mathbf{g}\|, \quad l \in \{1, \dots, 4\}, \quad (12)$$

where $\mathbf{a}_l = [a_l^x, a_l^y, a_l^z]^\top$, and which can be solved in closed form. We choose a positive real-number value out of the two possible solutions in order to correctly assign the acceleration values. New per-axis acceleration limits \mathbf{a}_{\max} and \mathbf{a}_{\min} are then determined as

$$\begin{aligned} a_{\max}^i &= \min\{\beta_l a_l^i \mid a_l^i > 0\}, \quad i \in \{x, y, z\}, \\ a_{\min}^i &= \max\{\beta_l a_l^i \mid a_l^i < 0\}, \quad l \in \{1, \dots, 4\}. \end{aligned} \quad (13)$$

The described process does not guarantee that $\|\mathbf{a}^T\| = a_{\max}^T$ after recomputing the trajectory with the new per-axis acceleration bounds (13). Yet as shown in following sections, after few iterations of the algorithm we can approximate the acceleration distribution so that $\|\mathbf{a}^T\| - a_{\max}^T < \varepsilon_a$ holds for a predefined threshold $\varepsilon_a \in \mathbb{R}$. This is also the stopping criteria of the algorithm, described in Alg. 1.

Algorithm 1: Limited Thrust Decomposition

In : \mathbf{X}_0 - trajectory initial conditions, ε_a - precision, a_{\max}^T - maximal thrust acceleration

Out: Π - resulting trajectory

```

1  $\mathbf{a}_{\max}, \mathbf{a}_{\min} \leftarrow \text{getInitAccLimits}(a_{\max}^T)$  ▷ (8)
2  $\Pi \leftarrow \text{pmmTraj3D}(\mathbf{X}_0, \mathbf{a}_{\max}, \mathbf{a}_{\min})$ 
3 while  $|\max\{\|\mathbf{a}_l^T\|\} - a_{\max}^T| > \varepsilon_a$  do
4    $\mathbf{d}_1, \dots, \mathbf{d}_4 \leftarrow \text{getDrag}()$  ▷ (10)
5    $\beta_1, \dots, \beta_4 \leftarrow \text{calculateScalingFactors}()$  ▷ (12)
6    $\mathbf{a}_{\max}, \mathbf{a}_{\min} \leftarrow \text{getNewAccLimits}()$  ▷ (13)
7   Update  $\Pi$  given  $\mathbf{a}_{\max}, \mathbf{a}_{\min}$ 

```

When employed for the velocity constrained bang-singular-bang policy, no additional steps are needed, as the same acceleration bounds are considered. However, an additional challenge involves distributing the maximum velocity norm constraint v_{\max} across individual axes. To address this, the per-axis velocity constraint $\mathbf{v}_m = [v_m^x, v_m^y, v_m^z]^\top$ is adjusted in each iteration according to

$$\mathbf{v}_m = \frac{\mathbf{v}^*}{\|\mathbf{v}^*\|} \cdot v_{\max}, \quad (14)$$

where $\mathbf{v}^* = [v^{x*}, v^{y*}, v^{z*}]^\top$, is a vector of largest velocities attained for each axis, $v^{i*} = \max_{t \in [0, T_s]} |v^i(t)|$ for $i \in \{x, y, z\}$.

D. Velocity Optimization

In the previous sections, we assumed that all the states necessary for PMM trajectory planning are known. However, for a multi-waypoint trajectory, this is generally not the case. Usually, we have full knowledge about the start and end states; but the via-waypoints are defined only by their positions. The problem of finding optimal velocities $\mathbf{v}_i \in \mathbb{R}^n$ for all via-waypoints of a PMM trajectory that minimize the trajectory duration $T_{\Pi} : \mathbb{R}^n \rightarrow \mathbb{R}$ can be formally written as

$$\{\mathbf{v}_1^*, \dots, \mathbf{v}_n^*\} = \arg \min_{\mathbf{v}_1, \dots, \mathbf{v}_n \in \mathbb{R}^n} T_{\Pi}(\mathbf{v}_1, \dots, \mathbf{v}_n), \quad (15)$$

where n is the number of via-waypoints of the given path from which the trajectory is computed. The problem is also subjected to all the trajectory feasibility constraints described

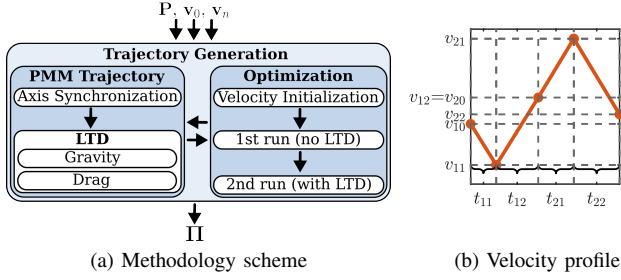


Fig. 2. PMM trajectory generation scheme (a) and the visualization of a two-segment single-axis trajectory velocity profile (b).

in Sec. III-A and Sec. III-B. To solve (15), we propose a new iterative approach based on the gradient method [22], previously used to optimize polynomial trajectories [7].

We first demonstrate the core ideas on a two-segment trajectory with defined start and end states and one via-waypoint position. The velocity profile of such a single-axis trajectory is shown in Fig. 2b. The Sec. III-A notation is adjusted, where for the second segment $v_0 = v_{12}$. The trajectory duration is then equal to

$$T_{\Pi} = T_1 + T_2 = t_{11} + t_{12} + t_{21} + t_{22}, \quad (16)$$

where T_1 and T_2 are the corresponding segment durations as defined in (3). The problem (15) is then reduced to

$$v_{12}^* = \arg \min_{v_{12} \in \mathbb{R}} T_{\Pi}(v_{12}) = \arg \min_{v_{12} \in \mathbb{R}} T_1(v_{12}) + T_2(v_{12}). \quad (17)$$

The gradient of the objective function $T_{\Pi}(v_{12})$ is then

$$\nabla T_{\Pi}(v_{12}) = \frac{\partial T_{\Pi}}{\partial v_{12}} = \frac{\partial T_1}{\partial v_{12}} + \frac{\partial T_2}{\partial v_{12}}, \quad (18)$$

where the partial derivatives of a segment's duration with respect to its start and end velocity are used. Having a differentiable objective function and its gradient, we can apply the gradient method to the problem (17) and formulate the update step for a given step size $\alpha > 0$ as

$$v_{12_{k+1}} = v_{12_k} - \alpha \nabla T_{\Pi}(v_{12_k}). \quad (19)$$

Velocity optimization is then computed by iteratively optimizing an initial estimate of the unknown velocity v_{12_0} using the update step (19) until the stopping criterion $|T_{\Pi}(v_{12_{k+1}}) - T_{\Pi}(v_{12_k})| < \varepsilon_T$ is satisfied for a given threshold $\varepsilon_T > 0$.

To account for the bounded segment duration for all axes in a multidimensional case, we distinguish between the following roles of single-axis trajectories: the slowest trajectory (1) dictating the total time will be called an M segment; the remaining synchronization segments will be labeled S segments. Since S segments are slowed down, performing optimization of the boundary velocity v_{12} does not yield improvement in the trajectory time when both consecutive segments are synchronization trajectories (S-S case). The M-S and S-M cases are treated analogously; we showcase only the S-M case. As the S segment has a constant duration T_S , the gradient (18) is reduced to

$$\nabla T_{S-M}(v_{12}) = \frac{\partial T_{S-M}}{\partial v_{12}} = \underbrace{\frac{\partial T_S}{\partial v_{12}}}_0 + \frac{\partial T_M}{\partial v_{12}} = \frac{\partial T_M}{\partial v_{12}}, \quad (20)$$

where T_M is the M segment duration. The S segment places bounds on the final updated velocity as its feasibility must be

preserved, which means that the acceleration scale is within the defined interval $\gamma \in (0, 1]$. We do this by fixing $\gamma = 1$ and solving the S segment system of equations described in Sec. III-B for the unknown velocity v_2 , which can be done in closed form. There are four possible solutions. The ones that meet the trajectory feasibility conditions presented in Sec. III-B and are closest to the current boundary velocity v_{12_k} in Euclidean distance are selected as the lower and upper bounds. We refer to S segment velocity bounds computation as **getSLim** in Alg. 2. The M segment also places bounds on the velocity update, which are determined by the real-world requirement on the non-negative sub-segment durations. To find those, we define the following modified trajectory duration function

$$T_{\Pi}^{abs} = |t_1| + |t_2|. \quad (21)$$

A real absolute value function $f(x) = |x|$ is continuous and differentiable everywhere except for $x = 0$, $x \in \mathbb{R}$, which is precisely where x changes its sign. By finding the non-differentiable points of the function (21), we can find the values of the boundary velocity, for which the sub-segment durations change their sign and cause trajectory infeasibility. This is done by finding the six undefined points of the partial derivative of (21) with respect to the boundary velocity v_{12} . The relevant ones are selected analogously to the S segment case and returned by the method **getMLim** in Alg. 2. For the M-M case, the velocity update remains according to (19), and is subjected to bounds determined by both the M segments as described above. The described approach can be analogously applied to bang-singular-bang trajectories, with an additional constraint on the velocity $|v_{12}^{i*}| \leq \max(|v_{11}^i|, |v_{21}^i|)$, $i \in [x, y, z]$ to ensure that the maximum velocity constraint is not exceeded.

Extending the concept to a multi-segment trajectory results in the following iterative method illustrated in Fig. 2a. First, the unknown velocities are initialized using **initVel** method in Alg. 2. To obtain the initial velocity heading at each waypoint, we take the previous and next heading vectors \mathbf{h}_p and \mathbf{h}_n . Given the angle θ between them and the distances to the previous and next waypoints l_p and l_n , the \mathbf{h}_p is rotated around the vector $\mathbf{h}_p \times \mathbf{h}_n$ towards \mathbf{h}_n by the angle

$$\theta_n = \frac{1-r}{2} \cdot \theta + \frac{r \cdot l_p}{l_p + l_n} \cdot \theta, \quad (22)$$

where $r = 0.6$ limits the rotation angle interval. The velocity norm is estimated by assuming zero velocities in the previous and next waypoints and computing the maximal reachable velocity, which is then scaled according to θ to account for the sharpness of the turn. Once the velocities are initialized, at every iteration, starting from one end of the multi-segment trajectory and going toward the other end, we take two neighboring trajectory segments, apply the per-axis velocity update steps to their boundary velocity, and update them accordingly. The two-segment window then shifts by one segment. This is repeated until the end of the trajectory is reached, as shown in Alg. 2. The order of the velocity updates is changed in every iteration for better convergence.

The per-axis velocity optimization can cause a trajectory segment duration increase due to a role change between the

single-axis trajectories caused by the axis synchronization. Therefore, we check for the duration increase after each update of a two-segment trajectory. If it occurs, the axes that caused it are determined by tracking the segment role changes (`getChangedAxes` method in Alg. 2), the corresponding per-axis gradient method update step size is reduced by a reduction factor $\eta \in (0, 1)$ as $\alpha_i = \eta \alpha_i$, and the update process repeats. This is done until either the duration decreases or the update step α_i is reduced below a threshold $\zeta \in \mathbb{R}$. The update for the given i -axis is then terminated using $\alpha_i = 0$. After each window shift, the update steps for all axes are reinitialized to a given initial value $\alpha_{\text{init}} > 0$.

Algorithm 2: PMM Trajectory Velocity Optimization

In : \mathbf{P} - set of path waypoints, $(\mathbf{v}_0, \mathbf{v}_n)$ - start and end velocity
Global: α - step size, η - reduction factor, ζ - reduction threshold;
 ε_T - time threshold
Out: Π - Optimized trajectory

```

1  $\mathbf{V}_0 \leftarrow \text{initVel}(\mathbf{P})$ 
2  $\Pi_0 \leftarrow \text{pmmTraj3D} \forall$  segments using  $\mathbf{V}_0$  and  $\mathbf{P}$ 
3 for each iteration  $k \in \{1, 2, \dots\}$  do
4    $\mathbf{V}_k \leftarrow \mathbf{V}_{k-1}$ 
5   Switch order  $\in \{\{1, \dots, n-2\}, \{n-2, \dots, 1\}\}$ 
6   for each segment  $s \in \text{order}$  do
7      $\alpha \leftarrow [\alpha, \alpha, \alpha]^T$  ▷ Reinitialize step size
8     for each axis  $i \in \{0, 1, 2\}$  do
9        $v_{12} \leftarrow \mathbf{V}_{k-1}[s][i]$ 
10       $\Pi_1^i, \Pi_2^i \leftarrow \Pi_k[s-1][i], \Pi_k[s][i]$ 
11      if  $\Pi_1^i$  is  $S$  and  $\Pi_2^i$  is  $S$  then
12        continue
13      else if  $\Pi_1^i$  is  $M$  and  $\Pi_2^i$  is  $M$  then
14         $v_{12_k} \leftarrow v_{12} - \alpha[i] \nabla T_{\Pi}(v_{12})$  ▷ (18)
15         $v_{12_B} \leftarrow \text{getMLim}(\Pi_1^i), \text{getMLim}(\Pi_2^i)$ 
16      else if  $\Pi_1^i$  is  $M$  and  $\Pi_2^i$  is  $S$  then
17         $v_{12_k} \leftarrow v_{12} - \alpha[i] \nabla T_1(v_{12})$  ▷ (20)
18         $v_{12_B} \leftarrow \text{getSLim}(\Pi_2^i), \text{getMLim}(\Pi_1^i)$ 
19      else if  $\Pi_1^i$  is  $S$  and  $\Pi_2^i$  is  $M$  then
20         $\text{Analogous to the previous case}$  ▷ (20)
21      Clip  $v_{12_k}$  given  $v_{12_B}$  and  $\mathbf{V}_k[s][i] \leftarrow v_{12_k}$ 
22      Update  $\Pi_1, \Pi_2$  using pmmTraj3D for  $\mathbf{V}_k[s]$ 
23      if  $(T_{1_k} + T_{2_k}) > (T_{1_{k-1}} + T_{2_{k-1}})$  then
24         $j \leftarrow \text{getChangedAxes}()$ 
25         $\alpha[j] \leftarrow \eta \alpha[j] \quad \forall j$ 
26        if  $\exists j \text{ s.t. } \alpha[j] < \zeta$  then
27           $\alpha[j] \leftarrow 0$ 
28        Update  $\Pi_1, \Pi_2$  for  $\mathbf{V}_{k-1}[s]$ 
29         $s \leftarrow s - 1$ 
30      else
31         $\Pi_k[s-1][i], \Pi_k[s][i] \leftarrow \Pi_1, \Pi_2$ 
32    if  $|T_{\Pi_k} - T_{\Pi_{k-1}}| < \varepsilon_T$  then
33      break
```

Including the Alg. 1 in the `pmmTraj3D` in Alg. 2 leads to early termination in local minima in some cases, as the assumption of constant per-axis acceleration limits is used in Alg. 2. Therefore, we run the optimization in two steps. First, the Alg. 2 is run with constant acceleration limits and the resulting trajectory is then recomputed using the Alg. 1. In the second step, Alg. 2 is run with incorporated Alg. 1.

IV. RESULTS

The proposed approach is verified in the following experiments. We compare the duration of two-waypoint trajectories generated by our LTD approach against the state-of-the-art method with fixed per-axis constraints [12]. Effects of LTD

coupled with the inclusion of external gravitational and drag forces on trajectory duration and tracking error are shown through an ablation study. Our gradient-based multi-waypoint trajectory optimization is evaluated against the state-of-the-art sampling-based Cone Refocusing [11] and time-optimal planner for full quadrotor model [4] in terms of computational time and trajectory duration. Finally, we verify the method in real-world flights in an outdoor environment, where we compare the tracking errors when following trajectories generated by our method and trajectories generated for a full quadrotor model [4].

All methods are implemented in C++ and simulation experiments are run on AMD Ryzen 7 6800HS CPU, with up to 4.7 GHz. Parameters $\alpha = 10$, $\zeta = 0.2$, $\varepsilon_T = 10^{-3}$ were used for the first step of the Alg. 2, and values $\alpha = 35$, $\zeta = 0.1$, $\varepsilon_T = 10^{-2}$ were adjusted for the second run. Precision $\varepsilon_a = 10^{-2}$ was used in Alg. 1. The UAV used in this study, shown in Fig. 1, has a mass of 1.21 kg, maximum collective thrust of 68 N, and estimated drag coefficients $\delta^x = 0.28$, $\delta^y = 0.35$, and $\delta^z = 0.7$ obtained by analysis of flight data aided with real-time kinematic (RTK) GPS and using various constant speed flights. It is equipped with Kadas VIM3 on-board computer and a civilian-grade GNSS capable of withstanding accelerations up to 4g. Considering these factors, we conducted the experiments with maximum total thrust limited to $a_{\text{max}}^T = 3.5g$, which is equivalent to 10.5 N per motor. We use the MRS UAV system [23], [24] for both simulation and real-world validation of the proposed method. The trajectories were tracked using NMPC used in [4] to track time-optimal trajectories for a full quadrotor model. NMPC generates the desired body rates and collective thrust, subsequently sent to the PX4 flight controller.

A. Trajectory planning evaluation

1) *Single-segment trajectory:* To assess the impact of our LTD approach, we evaluate the average duration of single-segment trajectories. Start and end positions are randomly sampled within a $(15 \text{ m})^3$ spatial cuboid, while start and end velocities are sampled within the interval $[-\frac{v_{\text{max}}}{\sqrt{3}}, \frac{v_{\text{max}}}{\sqrt{3}}]$ for each axis. The evaluation involves generating 100 trajectories for each combination of velocity and acceleration limits.

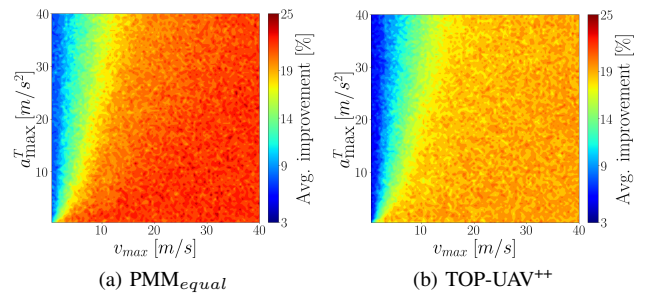


Fig. 3. Improvement of LTD compared to $\text{PMM}_{\text{equal}}$ and TOP-UAV^{++} .

Figure 3 shows how much LTD reduces trajectory duration compared to PMM using equal per-axis constraints ($\text{PMM}_{\text{equal}}$) and TOP-UAV^{++} [12]. The reduction is expressed as $(T_{\text{other}} - T_{\text{LTD}})/T_{\text{other}}$, where T_{other} is the duration of the trajectory from the other methods. For a fair comparison, we set $g = 0$, $\mathbf{D} = \mathbf{0}$. Results show that LTD shortens the

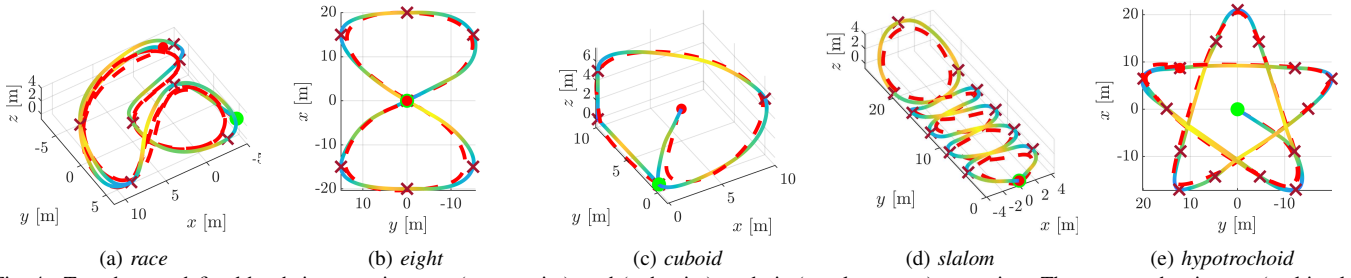


Fig. 4. Tested maps defined by their respective start (green point), end (red point), and via (purple crosses) waypoints. The computed trajectory (multi-color line) and the recorded UAV positions from the real-world flight (red dashed line) tracking the trajectories are displayed.

trajectory duration by 5% to 25% compared to $\text{PMM}_{\text{equal}}$, and by 3% to 22% compared to TOP-UAV^{++} . The most significant improvement is observed in scenarios with high velocity and acceleration, aligning with our focus on agile flight. In terms of runtimes, the $\text{PMM}_{\text{equal}}$ approach is the fastest, averaging 464 ns per trajectory. TOP-UAV^{++} takes about 980 ns and LTD averages $2.3 \mu\text{s}$ per trajectory, which corresponds with average five iterations of LTD to converge. Despite a slight increase in runtime, LTD remains suitable for online computation, while significantly reducing trajectory duration, especially in agile flight conditions.

2) *Multi-waypoint trajectory*: The proposed Gradient Descent (GD) approach for PMM trajectory optimization in Alg. 2 was compared with the sampling-based cone-refocusing (CR) method [11] and CPC approach [4] which considers a full dynamical model of the UAV. The five maps used for the comparison are shown in Fig. 4. Since CR does not consider drag, we excluded it from this experiment for both our approach and CPC. The tolerance of missing the waypoint for CPC was set to 0.3 m. The resulting computational times and trajectory durations are shown in table Table I. Our method outperforms CR in 2/5 cases in terms of trajectory duration, by 3.15% on average. In the remaining cases, it produces trajectories that are, on average, only 2.25% slower. This is due to the per-axis velocity optimization, where in some cases, the velocity in a waypoint for a given axis is not adjusted due to the adjacent trajectory segments being S-segments, even though an adjustment would decrease the trajectory duration in the global scope. Consequently, better results are achieved for the two trajectories, which are planar and the change in position of the waypoints for the main two trajectory axes are of a similar magnitude. Without considering drag, the trajectories generated by the CPC algorithm are slower in all tested scenarios. The full dynamical model contains constraints which PMM violates, leading to CPC's slower trajectories. However, during flight, NMPC enforces all of CPC's constraints, even when tracking PMM trajectories. Notably, PMM_{GD} planner utilized 99.92% of available collective thrust on average throughout all 5 trajectories, dropping to 95.82% when drag is considered. Looking at the computational times of all compared methods, the main contribution of our approach is evident. The CPC algorithm takes hours to converge, whereas our method can generate a trajectory in milliseconds or even tenths of milliseconds for some trajectories, up to two orders of magnitude faster than CR method. The computational times under 10 ms prove our approach suitable for real-time trajectory planning, essential for real-world deployment in presence of uncertainties, a capability not achievable with

current state-of-the-art methods.

TABLE I
MULTI-WAYPOINT TRAJECTORY OPTIMIZATION

map (waypoints)	CPC [4]		PMM_{CR} [11]		PMM_{GD}	
	c.t.[s]	T_s [s]	c.t.[ms]	T_s [s]	c.t.[ms]	T_s [s]
race (19)	4320	17.37	376	16.32	6.21	16.48
eight (9)	1390	9.46	96	9.14	1.28	8.93
cuboid (6)	225	5.89	74.6	4.84	0.78	5.10
slalom (13)	977	12.20	154	11.05	0.58	11.18
hypotrochoid (22)	9720	16.13	193	16.48	5.26	15.82

B. Ablation study

The significance of using acceleration norm constraint instead of per-axis limits, as well as considering gravity and drag-induced acceleration at high speeds is demonstrated through an ablation study. The study analyzes their effects on computational time, trajectory duration, and tracking root mean square error (RMSE). The results, shown in Table II, consider the methods in the following order of columns: $\text{PMM}_{\text{equal}}$ and LTD without any external forces, $\text{PMM}_{\text{equal}}$ and LTD with gravity, and LTD with both gravity and drag-induced acceleration. As observed in Sec. IV-A1, the LTD approach generates significantly faster trajectories than $\text{PMM}_{\text{equal}}$, albeit with a higher computational time. The fastest trajectories for both $\text{PMM}_{\text{equal}}$ and LTD are recorded when neither gravity nor drag is considered, as expected since the entire thrust can be utilized. Yet, it directly causes a significantly higher RMSE. Incorporating gravity and drag-induced acceleration results in a reduction of RMSE, bringing LTD with drag nearly on par with $\text{PMM}_{\text{equal}}$ in terms of RMSE, while still generating significantly faster trajectories.

C. Real-world evaluation

Finally, we validate our approach in real-world flights by deploying our UAV in an open outdoor environment, utilizing RTK GPS for state estimation. We record RMSEs (column RW) for our PMM approach both with modeling drag (PMM_{GD} w/ drag) and without it (PMM_{GD}), as well as for CPC algorithm [4], in Table III. Table III also includes computational times for our PMM methods on the embedded computer onboard our UAV, showing that the computation takes around 3.5 times longer, up to 60 ms, which remains suitable for online deployment. As anticipated, PMM without drag modeling exhibits the largest tracking error across all trajectories. However, PMM with drag-induced acceleration outperforms the CPC algorithm in 3 out of 5 cases, with very competitive results in the remaining two. The most significant advantages of our approach are observed in trajectories covering larger areas, *eight* and *hypotrochoid*. These

TABLE II
IMPACT OF GRAVITY, LTD AND DRAG ON PMM_{GD} COMPUTATIONAL TIME, TRAJECTORY DURATION AND TRACKING RMSE [m]

map	$PMM_{equal, g=0}$			LTD, $g=0$			PMM_{equal}			LTD			LTD w/ drag		
	c.t.[ms]	T_s [s]	RMSE	c.t.[ms]	T_s [s]	RMSE	c.t.[ms]	T_s [s]	RMSE	c.t.[ms]	T_s [s]	RMSE	c.t.[ms]	T_s [s]	RMSE
race	0.24	19.34	0.60	6.00	16.00	0.67	0.42	21.30	0.60	6.21	16.48	0.65	11.9	18.51	0.63
eight	0.05	11.17	0.89	1.2	8.75	1.04	0.05	12.35	0.85	1.28	8.93	1.01	5.32	10.44	0.90
cuboid	0.03	6.11	0.61	0.31	4.97	0.74	0.03	6.75	0.54	0.78	5.10	0.73	1.06	5.79	0.62
slalom	0.12	13.36	0.55	0.30	11.00	0.64	0.12	14.87	0.52	0.58	11.18	0.62	2.7	12.40	0.57
hypotrochoid	0.35	20.10	0.79	5.25	15.46	1.15	0.32	21.86	0.77	5.26	15.82	1.04	18.6	18.51	0.85

trajectories reach significantly higher velocities, leading to increased drag. This further highlights our approach in agile flight conditions. To verify obtained results, we perform five flights per method per map in simulation to exclude external factors like wind and state estimation errors. The results, shown in the SIM column of Table III, align with real-world findings. They indicate that trajectory duration has the most significant impact on RMSE, suggesting minimal benefit in computing a computationally intensive trajectory for a full model. Instead, our significantly faster trajectory planner that generates trajectories with comparable tracking errors proves to be a more efficient choice.

TABLE III
TRACKING RMSE [m] COMPARISON WITH STATE-OF-THE-ART

map	CPC [4] w/ drag			PMM_{GD}				PMM_{GD} w/ drag			
	T_s [s]	SIM	RW	c.t.[ms]	T_s [s]	SIM	RW	c.t.[ms]	T_s [s]	SIM	RW
race	18.55	0.56	1.05	25	16.48	0.63	1.07	40.7	18.51	0.62	1.04
eight	10.04	0.92	1.84	5.1	8.93	1.00	2.97	17.4	10.44	0.90	1.48
cuboid	6.36	0.55	0.93	3.2	5.10	0.72	1.04	3.5	5.79	0.62	1.00
slalom	13.42	0.39	0.88	2.3	11.18	0.63	1.08	9.0	12.40	0.57	0.92
hypotrochoid	16.59	0.99	3.62	20.8	15.82	1.03	4.01	61.8	18.51	0.87	1.60

V. CONCLUSIONS

We introduced novel approach capable of planning minimum-time multi-waypoint trajectories for agile flight in real time. Our gradient-based method optimizes apriori unknown velocities at the waypoints and converges to optimal solutions within milliseconds. We proposed using acceleration norm constraints instead of per-axis constraints through the Limited Thrust Decomposition algorithm. This enables the drone to utilize its maximum collective thrust and improves the duration of single-segment point-mass trajectories by up to 25%. We directly consider gravitational force to fully utilize the collective acceleration produced by the motors. Notably, our work is the first to address drag compensation in the point-mass model, demonstrating the benefits when flying at high velocities, through an ablation study. We verified our approach in real-world flights when using NMPC, where trajectories with accelerations of up to 3.5g and velocities over 100 km/h, generated within milliseconds, produced tracking errors similar to or smaller than the time-optimal trajectories found after several hours of computation by state-of-the-art methods utilizing a full quadrotor model.

REFERENCES

- [1] M. Atif, R. Ahmad, W. Ahmad, L. Zhao, and J. J. P. C. Rodrigues, "Uav-assisted wireless localization for search and rescue," *IEEE Systems Journal*, vol. 15, no. 3, pp. 3261–3272, 2021.
- [2] H. Ren, Y. Zhao, W. Xiao, and Z. Hu, "A review of uav monitoring in mining areas: current status and future perspectives," *International Journal of Coal Science & Technology*, vol. 6, pp. 320 – 333, 2019.
- [3] E. Kaufmann, L. Bauersfeld, A. Loquercio, M. Mueller, V. Koltun, and D. Scaramuzza, "Champion-level drone racing using deep reinforcement learning," *Nature*, vol. 620, pp. 982–987, 2023.
- [4] P. Foehn, A. Romero, and D. Scaramuzza, "Time-optimal planning for quadrotor waypoint flight," *Science Robotics*, vol. 6, no. 56, 2021.
- [5] Z. Zhou, G. Wang, J. Sun, J. Wang, and J. Chen, "Efficient and robust time-optimal trajectory planning and control for agile quadrotor flight," *IEEE Robotics and Automation Letters*, vol. 8, pp. 7913–7920, 2023.
- [6] T. Fork and F. Borrelli, "Euclidean and non-euclidean trajectory optimization approaches for quadrotor racing," *arXiv preprint arXiv:2309.07262*, 2023.
- [7] C. Richter, A. Bry, and N. Roy, "Polynomial trajectory planning for aggressive quadrotor flight in dense indoor environments," *Robotics Research*, pp. 649–666, 2016.
- [8] B. Zhou, J. Pan, F. Gao, and S. Shen, "Raptor: Robust and perception-aware trajectory replanning for quadrotor fast flight," *IEEE Transactions on Robotics*, vol. 37, no. 6, pp. 1992–2009, 2021.
- [9] R. Penicka and D. Scaramuzza, "Minimum-time quadrotor waypoint flight in cluttered environments," *IEEE Robotics and Automation Letters*, vol. 7, no. 2, pp. 5719–5726, 2022.
- [10] P. Foehn, D. Brescianini, E. Kaufmann, T. Cieslewski, M. Gehrig, M. Muglikar, and D. Scaramuzza, "Alphapilot," *Autonomous Robots*, vol. 46, no. 1, pp. 307–320, 2022.
- [11] A. Romero, R. Penicka, and D. Scaramuzza, "Time-optimal online replanning for agile quadrotor flight," *IEEE Robotics and Automation Letters*, vol. 7, no. 3, pp. 7730–7737, 2022.
- [12] F. Meyer, K. Glock, and D. Sayah, "Top-uav: Open-source time-optimal trajectory planner for point-masses under acceleration and velocity constraints," *IEEE/RSJ IROS*, 2023.
- [13] B. Zhou, F. Gao, L. Wang, C. Liu, and S. Shen, "Robust and efficient quadrotor trajectory generation for fast autonomous flight," *IEEE Robotics and Automation Letters*, vol. 4, no. 4, pp. 3529–3536, 2019.
- [14] D. Mellinger and V. Kumar, "Minimum snap trajectory generation and control for quadrotors," *IEEE ICRA*, 2011.
- [15] C. Qin, M. S. Michet, J. Chen, and H. H.-T. Liu, "Time-optimal gate-traversing planner for autonomous drone racing," 2024.
- [16] M. Hehn, R. Ritz, and R. D'Andrea, "Performance benchmarking of quadrotor systems using time-optimal control," *Autonomous Robots*, vol. 33, no. 1, pp. 69–88, Aug 2012.
- [17] R. Allen and M. Pavone, "A real-time framework for kinodynamic planning with application to quadrotor obstacle avoidance," *AIAA Guidance, Navigation, and Control Conference*, 2016.
- [18] F. Meyer and K. Glock, "Kinematic orienteering problem with time-optimal trajectories for multirotor uavs," *IEEE Robotics and Automation Letters*, vol. 7, no. 4, pp. 11402–11409, 2022.
- [19] A. Romero, S. Sun, P. Foehn, and D. Scaramuzza, "Model predictive contouring control for time-optimal quadrotor flight," *IEEE Transactions on Robotics*, vol. 38, no. 6, pp. 3340–3356, 2022.
- [20] D. P. Bertsekas, *Dynamic Programming and Optimal Control*, 3rd ed. Athena Scientific, 2007.
- [21] M. Faessler, A. Franchi, and D. Scaramuzza, "Differential flatness of quadrotor dynamics subject to rotor drag for accurate tracking of high-speed trajectories," *IEEE Robotics and Automation Letters*, vol. 3, no. 2, pp. 620–626, 2018.
- [22] S. Boyd and L. Vandenberghe, *Convex Optimization*. Cambridge University Press, 2004.
- [23] T. Baca, M. Petrlik, M. Vrba, V. Spurny, R. Penicka, D. Hert, and M. Saska, "The MRS UAV System: Pushing the Frontiers of Reproducible Research, Real-world Deployment, and Education with Autonomous Unmanned Aerial Vehicles," *Journal of Intelligent & Robotic Systems*, vol. 102, no. 26, pp. 1–28, 2021.
- [24] D. Hert, T. Baca, P. Petracek, V. Kratyk, R. Penicka, V. Spurny, M. Petrlik, M. Vrba *et al.*, "Mrs drone: A modular platform for real-world deployment of aerial multi-robot systems," *Journal of Intelligent & Robotic Systems*, vol. 108, no. 4, p. 64, 2023.